NUCL SCI TECH (2018) 29:80
https://doi.org/10.1007/s41365-018-0426-9

Preliminary experimental study on applicability of Lorentz force velocimetry in an external magnetic field

Yan-Qing Tan[1,4] · Run-Cong Liu[1] · Shang-Jun Dai[1] · Xiao-Dong Wang[1] · Ming-Jiu Ni[2] · Juan-Cheng Yang[2] · Nataliia Dubovikova[3] · Yurii Kolesnikov[3] · Christian Karcher[3]

Received: 9 August 2017 / Revised: 25 October 2017 / Accepted: 27 November 2017 / Published online: 25 April 2018

Abstract Lorentz force velocimetry (LFV) is a noncontact technique for measuring electrically conducting fluids based on the principle of electromagnetic induction. This work aims to answer the open and essential question of whether LFV can work properly under a surrounding external magnetic field (ExMF). Two types of ExMFs with different magnetic intensities were examined: a magnetic field with a typical order of 0.4 T generated by a permanent magnet (PM) and another generated by an electromagnet (EM) on the order of 2 T. Two forces, including the magnetostatic force between the ExMF and PM in the LFV, and the Lorentz force generated by the PM in LFV were measured and analyzed in the experiment. In addition, ExMFs of varying strengths were added to the LFV, and the location of the LFV device in the iron cores of the EM was considered. The experimental outcomes demonstrate that it is possible for a LFV device to operate normally under a moderate ExMF. However, the magnetostatic force will account for a high proportion of the measured force, thus inhibiting the normal LFV operation, if the ExMF is too high.

Keywords Lorentz force velocimetry · Electrically conducting fluids · Noncontact measuring technique · External magnetic field

This work was supported by the National Natural Science Foundation of China (No. 51374190) and the Major Equipment Fund of Chinese Academy of Sciences (No. YZ201567).

✉ Xiao-Dong Wang
xiaodong.wang@ucas.ac.cn

1 College of Materials Science and Opto-Electronic Technology, University of Chinese Academy of Sciences, Huairou District, Beijing 101408, China

2 School of Engineering Science, University of Chinese Academy of Sciences, Huairou District, Beijing 101408, China

3 Institute of Thermodynamics and Fluid Mechanics, Ilmenau University of Technology, P.O.Box 100565, 98684 Ilmenau, Germany

4 The Fifth Electronics Research Institute, Ministry of Industry and Information Technology, Guangzhou 510610, China

1 Introduction

Lorentz force velocimetry (LFV) is an electromagnetic noncontact flow measurement technique that was conceived in the 1960s [1, 2], and recent advancements suggest that it will soon be applicable to aluminum production, steel making, and universal fluids [3–5]. A review of the electromagnetic flow rate method based on the magnetohydrodynamics (MHD) theory led to the innovative development of the LFV [5–9], a contactless technology used to measure the flow rate of an electrically conducting fluid.

As the magnetic field plays an important role in the principle of LFV, involvement of a magnetic field other than that from the LFV is likely to change the measured result. The understanding and quantifying of this disturbance is essential in a number of areas. For example, in the area of fusion reactions [7, 10–14], liquid metals such as LiPb are used as media to realize heat and mass transfer from the reactors. The high magnetic field and its interaction with plasma, the so-called MHD effect, equivalently affect the normal impact of LFV. Another potential application lies in liquid metal processes, such as metallurgy and semiconductor crystal growth, where electromagnetic noise emits from metallurgical electromagnetic devices with different frequencies that can vary from very low to very high, and the prevalent induction phenomenon between the liquid metal and electromagnetic waves, including the thermo-electric effect (Seebeck effect), cannot be completely avoided [9]. However, to the best of our knowledge, the effects of an extra magnetic field on the LFV measurement have not been well studied.

In this paper, we studied the measurements taken by LFV under an external field. The results are quantified by attributing the result to the interactions among these factors: LFV, target flow, and external magnetic field (ExMF).

The magnetic field provided by the permanent magnet (PM) in the LFV can be determined by a magnetic dipole with dipole moment $\boldsymbol{m} = m\boldsymbol{e}_z$, whose magnetic field is given by Thess and Wang [6, 15]

$$\boldsymbol{B}(\boldsymbol{R}) = \frac{\mu_0}{4\pi}\left\{3(\boldsymbol{m}\cdot\boldsymbol{R})\frac{\boldsymbol{R}}{R^5}\frac{\boldsymbol{m}}{R^3}\right\}, \tag{1}$$

where $\boldsymbol{R}$ is the space vector from the magnetic dipole and $R=|\boldsymbol{R}|$. The eddy currents are induced in this electrically conducting fluid and can be computed from Ohm's law for a moving electrically conducting fluid,

$$\boldsymbol{J} = \sigma(-\nabla\Phi + \boldsymbol{u}\times\boldsymbol{B}), \tag{2}$$

where Φ is the electrical potential and $\boldsymbol{u}$ is the fluid velocity. The associated Lorentz force can be expressed as the interaction of the magnetic field and eddy current:

$$\boldsymbol{F} = \boldsymbol{J}\times\boldsymbol{B}, \tag{3}$$

which tends to break the flow; a reaction force ($\boldsymbol{F}' = \boldsymbol{F}$) is also exerted on the magnet itself tending to entrain the magnet in the flow direction. This force can be expressed in a scaling law,

$$\boldsymbol{F}' \sim \sigma\boldsymbol{u}\boldsymbol{B}^2, \tag{4}$$

where σ, $\boldsymbol{u}$, and $\boldsymbol{B}$ are the electrical conductivity, fluid velocity, and magnetic flux density, respectively. Equation (4) shows that the measured force acting upon on the magnetic-generating system F' is proportional to the velocity of the conducting fluid. The above discussion also applies to the interaction between the ExMF and target flow, as the ExMF exerts a magnetic field on the target flow in a similar way as the LFV. The Lorentz force from the ExMF acting on the target flow cannot be measured by the LFV; it is more likely to retard the flow if the ExMF is strong and more widely distributed in space. This phenomenon can be characterized by the magnetic Reynolds number, and it does not influence the measurement of the LFV. Aside from the ExMF-flow and LFV-flow interactions, the LFV also interacts with the ExMF. If the PM in the LFV is placed in an ExMF $\boldsymbol{B}_{\mathrm{ex}}$, it is capable of retaining its magnetism strength. We assumed that the ExMF around the PM area is uniform due to its small size. The potential energy in this case can be written as:

$$\boldsymbol{P} = \boldsymbol{B}_{\mathrm{ex}}\cdot\boldsymbol{m}. \tag{5}$$

Therefore, no net force, only a torque is applied on the PM, which can be written as:

$$\boldsymbol{\tau} = -\boldsymbol{B}_{\mathrm{ex}}\times\boldsymbol{m}. \tag{6}$$

The LFV only measures the "force" acting on the PM. The contribution to the measured force from the LFV–ExMF interaction in this case is dependent on the setup of the system. Yet, giving that the PM in the LFV is aligned perpendicular to the direction of the ExMF (see Fig. 3a, b), it is reasonable to conclude that the direction (the x direction in Fig. 3a) of the contributed force is perpendicular to the direction of the Lorentz force (the y direction in Fig. 3a).

2 Demagnetization of a PM under an ExMF

We must initially determine whether a PM block can sufficiently retain its magnetic strength without significant attenuation within an ExMF; if not, LFV cannot be applied in an electromagnetic environment. We thus performed a simple test by placing a PM in a high magnetic field (2 T) for a given duration. Figure 1 shows the surface magnetic field strength of a PM after exposure to a high magnetic field, and the liftoff distance is the distance from the surface of the PM. In Fig. 1a, A2 represents the perpendicular relationship of the PM magnetic field and two parallel current-carrying coil magnetic fields (ExMF, PM⊥ExMF), while in Fig. 1b A3 represents the parallel relationship between them (PM||ExMF). The magnetic field strength was clearly unchanged, even after durations of 10, 20, and 30 min. The results indicate that a PM can perfectly retain its strength in a relatively high 2 T magnetic field. In other words, the PM is not magnetized or demagnetized by the ExMF to some extent.

3 Sensor realization and testing in a "dry situation"

The experimental realization of an LFV sensor as described above is rather simple. As illustrated in Fig. 2, a rotary copper disk with a 25-mm diameter is used to mimic the movement of liquid metal. The Lorentz force acting upon the magnetic-force-generating system is measured using a force sensor. The magnet dimensions used in the LFV sensor are a diameter of 10 mm and a height of 5 mm, which is magnetized in the radial direction (shown in the small picture in Fig. 2). The distance between the ExMF

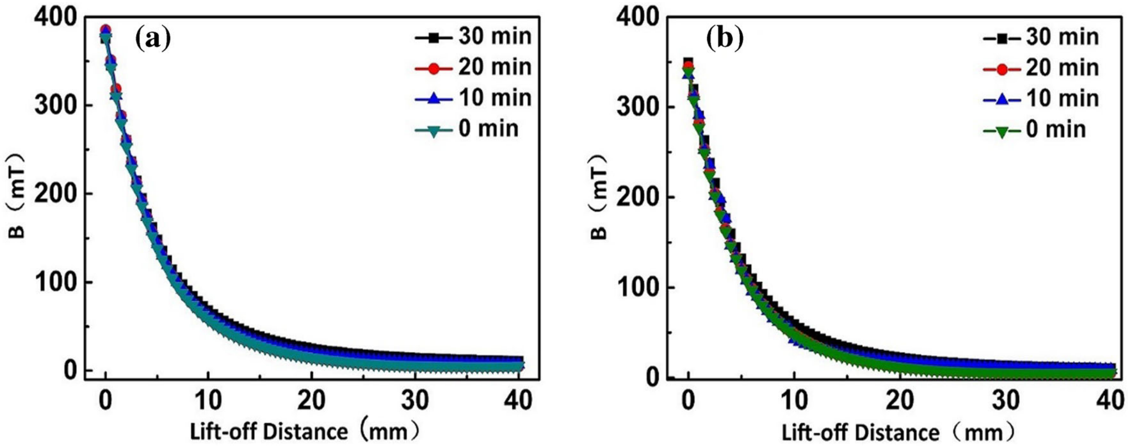

Fig. 1 (Color online) Magnetic field intensity attenuation of a PM used in LFV under an ExMF: **a** PM⊥ExMF and **b** PM||ExMF

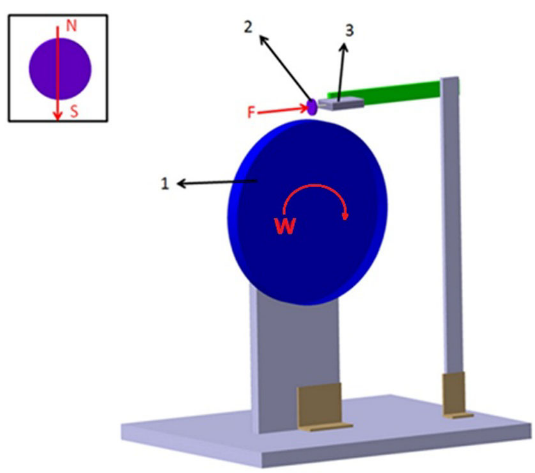

Fig. 2 (Color online) Schematic diagram of Lorentz force velocimetry (1—rotary copper disk; 2—permanent magnet; 3—force sensor)

and LFV device is 20 mm, controlled by a 3D micro-platform.

A DC motor is used to control the rotation rate, which is linear with a voltage exerted on the DC motor. The resulting rotation rates of the copper plate under voltages are represented in Table 1. The magnet and force sensor are held in place by a fixture made of Plexiglas. Nylon screws are used to fix each part of the holder to avoid interactions between any metal and the PM.

To mimic the ExMF, two types of magnetic-generating systems were used in this work, including a permanent system and an electromagnetic system, which are shown in Fig. 3a–d. In Fig. 3a, a permanent block magnet with dimensions 50 mm length, 50 mm width, and 10 mm height was used. To validate the practicality of LFV under a high magnetic field, we placed this LFV device in an electromagnet (EM) that can generate a magnetic field as high as 2 T [16]. As shown in Fig. 3d, the gap between the two iron cores is 80 mm and the LFV device is placed in the middle of the field and edge.

Table 1 Corresponding angular velocities of the rotating copper plate under different voltages

Voltage (V)	0	10	12	15
Angular velocities (r/min)	0	625	750	937.5

4 Results and discussion for a "dry situation"

4.1 Measured force of LFV without an ExMF

We initially performed a control experiment without any ExMF exerted on the LFV device. Figure 4 illustrates how the LFV process varies, with five stages divided by five points in time denoted as t_1 to t_5. When the copper plate is static, the measured force is zero, e.g., at t_1 and t_5. During the time between t_2 and t_5, the measured force increases as the copper plate rotates from w = 0–937.5 r/min. Only the Lorentz force can be measured because no ExMF is acting upon the force sensor. In total, the integral of the Lorentz force density over the magnetic-generating system exhibits three plateaus as the rotation rate of the copper disk increases. The relationship between the relative velocity and Lorentz force is shown in Fig. 4b. These results concur with those reported in Ref. [4], which states that the measured force is linear with respect to the relative velocity. Here, the nonzero intercept likely indicates the minimum measurable force.

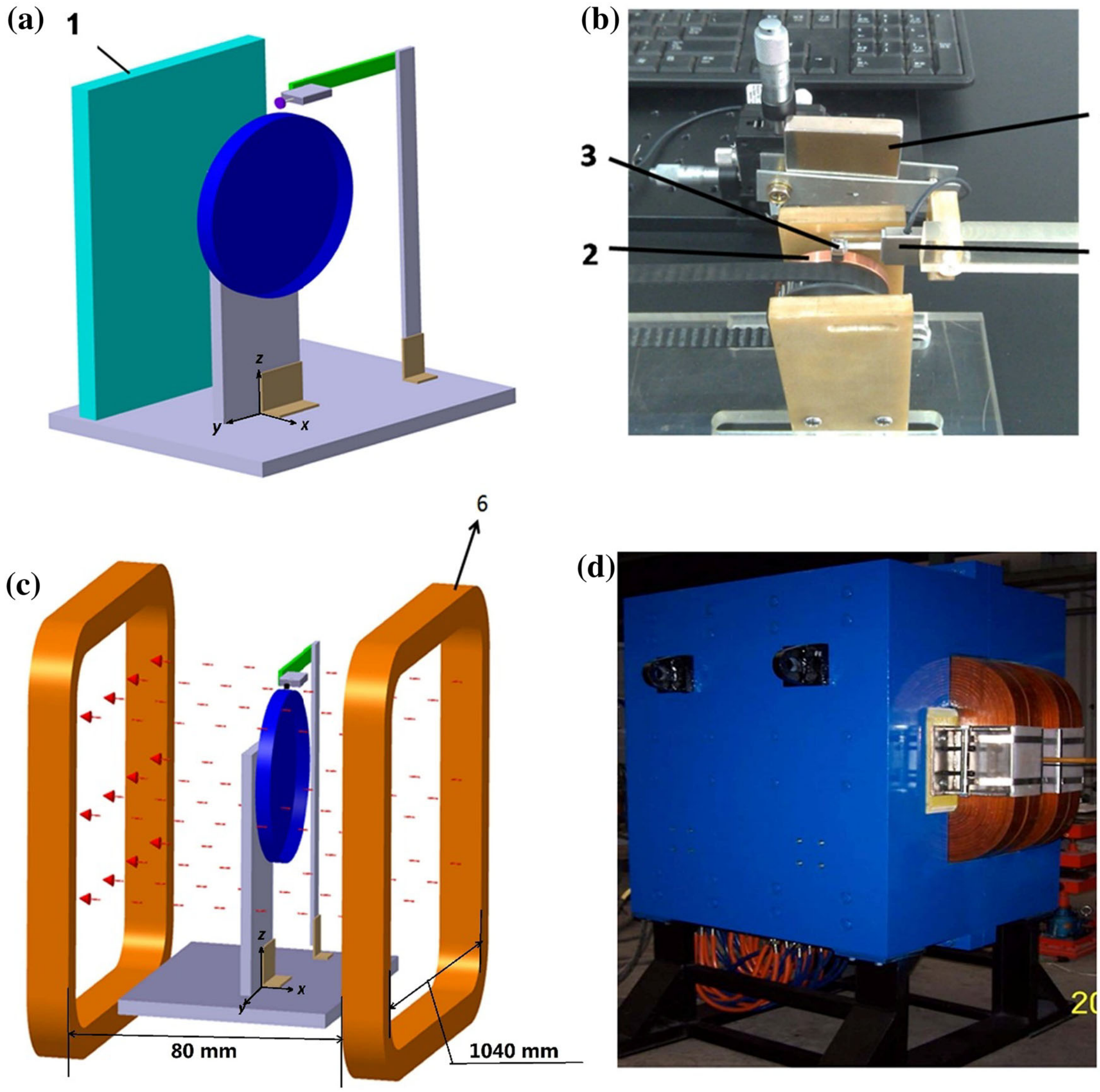

Fig. 3 (Color online) Schematic diagram and experimental devices of LFV under PM (**a**, **b**) and EM (**c**, **d**) mimicking an ExMF (1—external PM, 2—copper disk, 3—PM in LFV, 4—external PM, 5—force sensor, 6—external EM)

4.2 Measured force of LFV under PM mimicking external magnetic field

The results shown in Fig. 5 indicate an ExMF provided by an added PM (approximately 0.4 T near the sensor). This case also exhibits five stages that can be described by five points in time, from t_1 to t_5. At t_1 and t_5, the copper plate is static; thus, no Lorentz force is present and the total measured force is the magnetostatic force between the LFV and ExMF, labeled F_{MSF}. From t_1 to t_2, the measured force significantly increases as the PM moves closer to the LFV device, leading to an increase in F_{MSF}.

At t_2, the copper plate rotates with a constant velocity resulting in an increased measured force. At this stage, two elements of force are detected by the force sensor: F_{MSF} and the Lorentz force generated by the relative motion between the copper plate and PM in the LFV, $F_{\mathrm{LF\text{-}PM}}$. At t_3, the ExMF is removed, leading to the disappearance of F_{MSF}, thus causing a decrease in the measured force. For t_3–t_4, only the Lorentz force $F_{\mathrm{LF\text{-}PM}}$ generated by the PM can be detected by the force sensor. It is apparent in Fig. 5 that the measured force results can be divided into five stages, indicating that two elements of force can be identified by each other. Note that all of these forces, either magnetostatic or Lorentz, are vector quantities and are distributed in space, while the force measured by the LFV is the magnitude of the net force [5–9]. This point does not influence the general discussed problem. As discussed, the two elements of force acting in stage 3 are separately presented in stage 2 (F_{MSF}) and stage 4 ($F_{\mathrm{LF\text{-}PM}}$). Assuming the force measured in stage 3 is simply the combined forces of stages 2 and 4, the calculated angle between the two

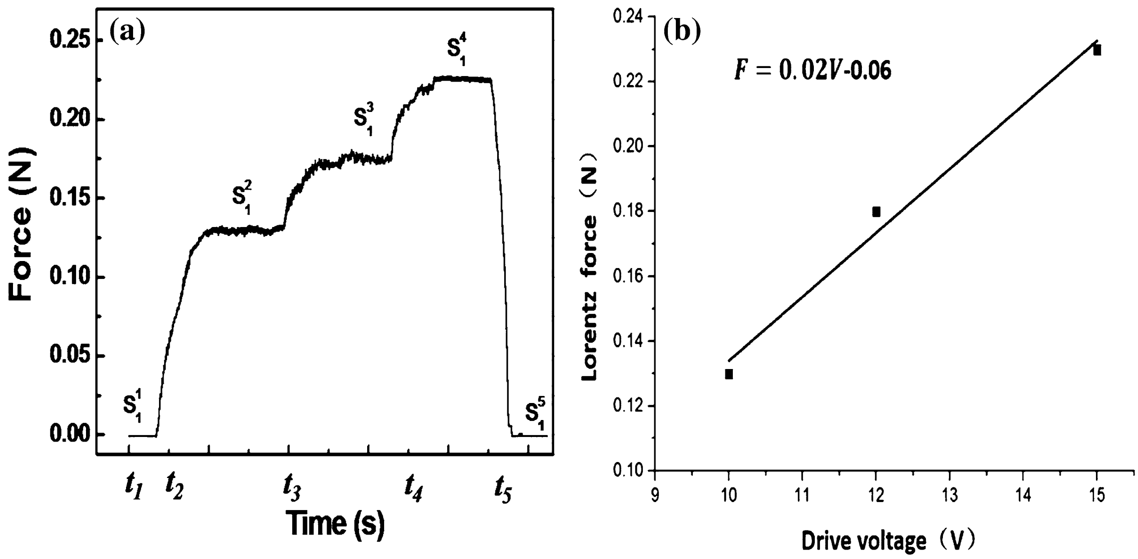

Fig. 4 **a** Different rotating speeds of the copper wheel as measured by LFV (S11: B = 0, w = 0 r/min; S12: B = 0, w = 625 r/min; S13: B = 0, w = 750 r/min; S14: B = 0, w = 937.5 r/min; and S14: B = 0, w = 0 r/min). **b** Measured Lorentz force at different driven voltage

Table 2 Measured Lorentz force and calculated angle between the two elements

B (T)	F_{MSF} (N)	$F_{LF\text{-}PM}$ (N)	$F_{MSF} + F_{LF\text{-}PM}$ (N)	Angle (°)
0.1079	0.064	0.150	0.173	100
0.2209	0.097	0.127	0.185	110
0.3902	0.123	0.121	0.171	89
1.008	0.138	0.115	0.147	N/A

force elements is 112° rather than 90°. The difference here could be the result from the decaying of the external PM.

4.3 Results and discussion for an electromagnet

Figure 6 shows the variation of the measured force under different ExMFs; the rotation velocity of the copper plate is w = 625 r/min. Figure 6a represents the force variation under 0.1079 T; the similarity of the five stages in

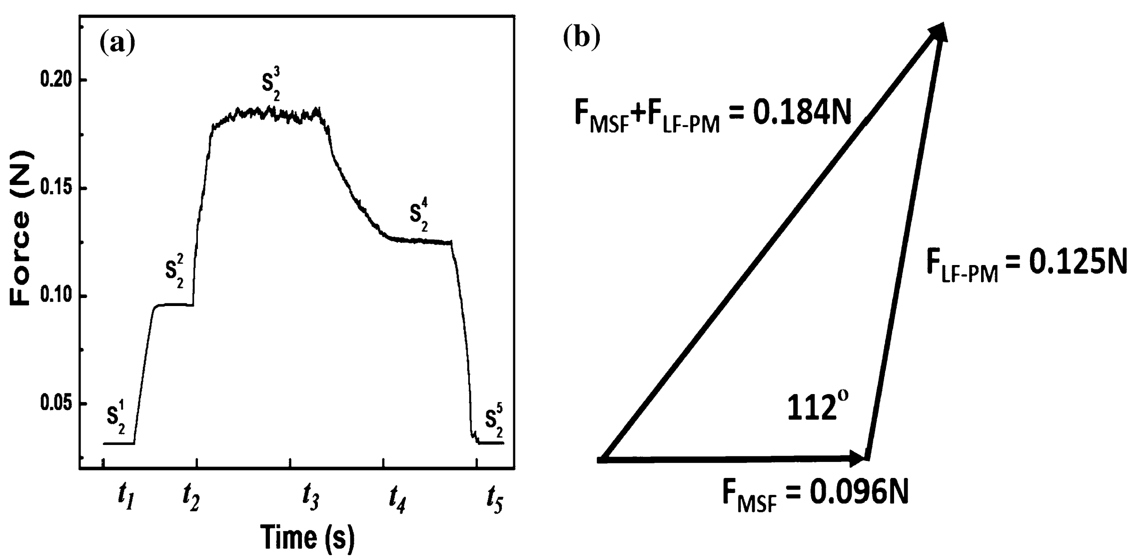

Fig. 5 **a** LFV operating in a PM magnetic field (S_2^1: B = 0 T, w = 0 r/min; S_2^2: B = 0.4 T, w = 0 r/min; S_2^3: B = 0.4 T, w = 625 r/min; S_2^4: B = 0, w = 625 r/min; S_2^5: B = 0 T, w = 0 r/min). The force measured from stage 2 (F_{MSF}), stage 3 (combined), and stage 4 ($F_{LF\text{-}PM}$) and its indicated relative directions

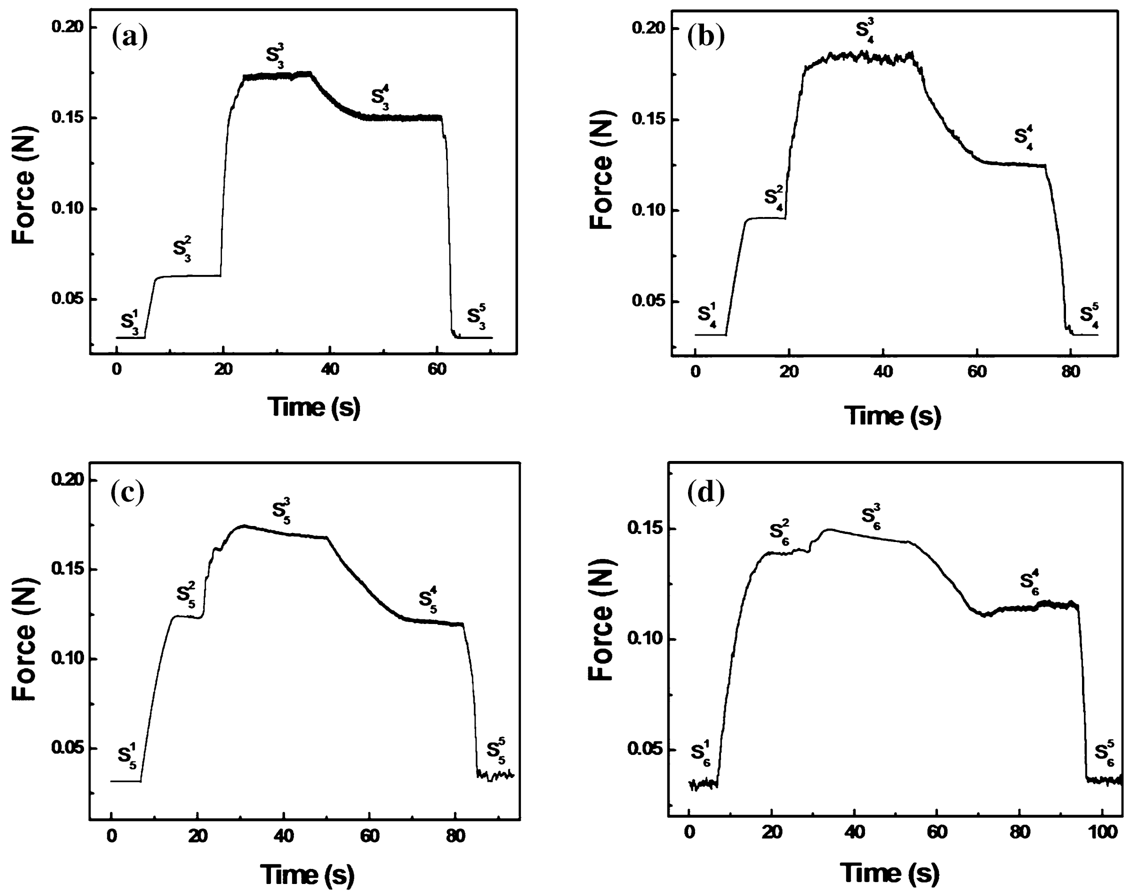

Fig. 6 Measured force variation for different ExMF values ($B = B_0 ey$). a–d correspond to 0.1079, 0.2208, 0.3902, and 1.008 T, respectively

this curve compared with Fig. 5 indicates that the force acted on the LFV under the EM is the same as the PM. At the S_3^1 and S_3^5 stages, the copper plate is static with no ExMF acting on it, whereas at stage S_3^2 an ExMF with magnitude of 0.1079 T is exerted. At stage S_3^3, the copper plate was rotated at a rate of 625 r/min, and the ExMF was then removed at stage S_3^4. Similarly, Fig. 6b–d shows the influence of different ExMFs. However, it is obvious in Fig. 6c, d that the plateaus decline at stages S_5^3 and S_6^3, perhaps caused by the significant static magnetic force between the ExMF and PM in the LFV, turning the initial direction of the PM and leading to the incline of these curves.

It is apparent that the measured force variation is similar to the force variation discussed above. All of the curves in the figures have three plateaus, indicating the five stages of the experimental process. The proportion of the magnetostatic force is greater in a higher ExMF. For example, with $B = 0.1079$ T, F_{MSF} is only 0.065 N (stage 1 from t_1 to t_2) and the total measured force is 0.178 N when the copper plate rotates (including F_{MSF}, $F_{LF\text{-}PM}$; the ratio of F_{MSF} is only 36.99%). As the ExMF increases to 0.2208, 0.3902, and 1.008 T, the ratios of F_{MSF} are 52.43, 71.93, and 93.88%, respectively. By performing the same analyses as we did in Sect. 4.2, when the ExMF is 0.1079, 0.2208, and 0.3902 T, the calculated angles between F_{MSF} and $F_{LF\text{-}PM}$ are 100°, 110°, and 90°, respectively (Table 2). These angles are close to the previous results and within a reasonable range.

However, when the ExMF is high (1.008 T), the force measured in stage 3 was close to that in stage 2 and does not agree with the above discussion. The possible reason for this inconsistency is that the ExMF, unlike the PM in LFV which only acts in a small area, distributes over all the space surrounding the copper plate in our system. Therefore, this ExMF is likely to significantly impede the motion of the copper plate, especially when it has a strong magnitude. When the drive voltage applied to the copper plate is same, the rotation speed in Fig. 6d can be dramatically lower, resulting in a similar Lorentz force measurement.

Furthermore, $F_{LF\text{-}PM}$ decreases as the ExMF increases, which is abnormal for the ideal situation. From t_3 to t_4, only $F_{LF\text{-}PM}$ can be detected by the force sensor. $F_{LF\text{-}PM}$ should be a constant because the same experimental condition as the ExMF was removed. As discussed in the first section, we know that the PM used in the LFV maintains its magnetization, even in a 2-T ExMF; therefore, the PM

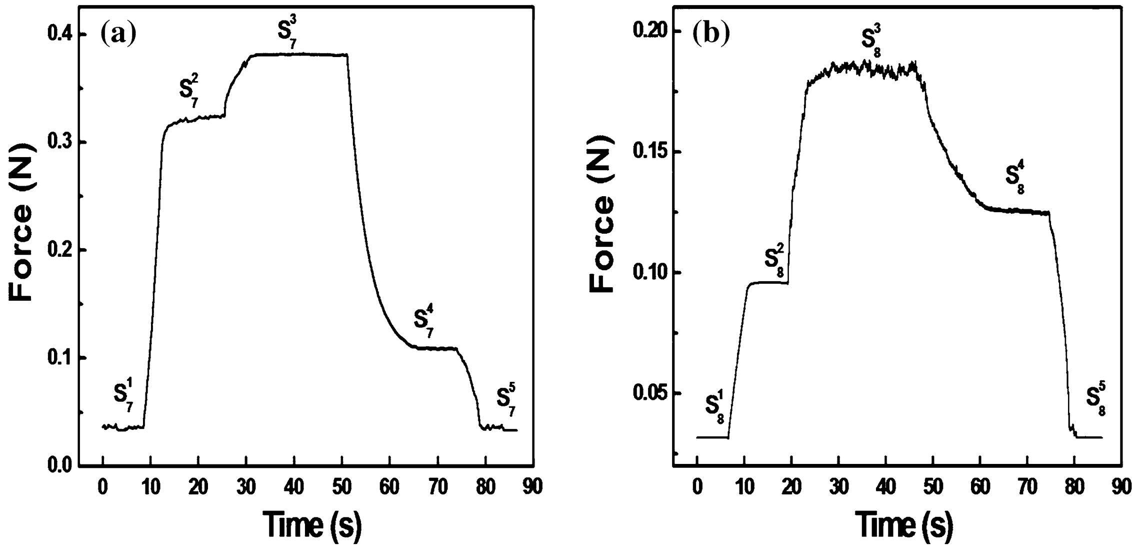

Fig. 7 Measured force variation curves as the LFV is placed at **a** the middle of the ExMF and **b** the edge of the ExMF

should not be demagnetized under these experimental conditions. Therefore, this result can be attributed to the increased F_{MSF} under a higher ExMF, acting on the PM and leading to a change in its magnetic direction.

We also considered the magnetic field distribution of the ExMF. We placed the LFV device at the middle of the EM gap (Fig. 7a) and at the edge of the EM gap (Fig. 7b); the results are presented in Fig. 7. Stages S_7^1, S_7^2, S_7^3, S_7^4, and S_7^5 represent different experiment conditions, e.g., $B = 0.2208$ T, $w = 0$ r/min at S_7^2, $B = 0.2208$ T, $w = 625$ r/min at S_7^3, and $B = 0$ T, $w = 625$ r/min at S_7^4. It is obvious that when the LFV device was placed in the middle of the gap, the ratio of F_{MSF} was much greater than that for the edge of the gap. This finding is similar to the results presented in Fig. 6 and indicates that the magnetic field in the middle of the ExMF gap is much stronger than the magnetic field at the edge. In fact, the magnetic field will be approximately uniform at any cross section for the core sections in the EM. However, at the edges the magnetic field lines are no longer confined by the core; thus, they "bulge" out beyond the outlines of the core before curving back to enter the next core material and the field strength is reduced in the gap [14].

5 Conclusion

In this study, we examined whether LFV can be applied in an ExMF. We answered this question from an experimental perspective for ExMFs generated by both a PM and an EM.

The practicality of using a PM in LFV has been successfully demonstrated based on the magnetic field attenuation behavior under a 2-T ExMF. Solid body experiments have been performed to provide a means for validating our assumption at various velocities in the range of $w = (625, 937.5$ r/min).Two contributions to the measured force were distinguished: the magnetostatic and Lorentz forces generated by the PM. These two forces acted on the magnetic-field-generated system at different stages and can be clearly discriminated in a relatively small ExMF.

As the ExMF increased, the proportion of the magnetostatic force increased, eventually exceeding 90% of the measured force for a 1-T magnetic field. According to the common surveying criterion, the measurement becomes more difficult when the force measured by the LFV yielded less than 1% of the magnetostatic force. Clearly, such situations with stronger ExMFs need further verification and careful study.

Future research will include a refinement of the experimental setup. An improved and optimized magnet system will be used, and the magnetic field intersection will be discussed. Moreover, the magnetostatic torque will be detected using another device to enable a quantitative analysis of the measured force. In this way, we will be able to investigate the effect of an ExMF on the LFV. The LFV should also be tested and verified with liquid metals, as well as an investigation concerning the MHD characteristics.

Acknowledgements The authors give their special thanks to Dr. André Thess for useful discussions.

References

1. J.A. Shercliff, *The theory of electromagnetic flow-measurement* (Cambridge University Press, Cambridge, 1962)
2. J.A. Shercliff, U. K. Patent GB 831,226, 23 Mar 1960
3. R.P. Uhlig, M. Zec, H. Brauer, A. Thess, Lorentz force Eddy current testing: a prototype model. J. Nondestruct. Eval. **31**, 357–372 (2012). https://doi.org/10.1007/s10921-012-0147-7
4. J. Priede, D. Buchenau, G. Gerbeth, Force-free and contactless sensor for electromagnetic flowrate measurements. Magnetohydrodynamics **45**, 451–458 (2009)
5. A. Thess, E.V. Votyakov, Y. Kolesnikov, Lorentz force velocimetry. Phys. Rev. Lett. **96**, 4 (2006). https://doi.org/10.1103/PhysRevLett.96.164501
6. A. Thess, E. Votyakov, B. Knaepen, O. Zikanov, Theory of the Lorentz force flowmeter. New J. Phys. **9**, 299 (2007)
7. X. Wang, R. Klein, Y. Kolesnikov, A. Thess, Application of Lorentz force velocimetry to open channel flow. Light Metals Tech. V **690**, 99–102 (2011). https://doi.org/10.4028/www.scientific.net/MSF.690.99
8. V. Minchenya, C. Karcher, Y. Kolesnikov, A. Thess, Tms, Lorentz force flowmeter in industrial application. Magnetohydrodynamics **45**, 459–466 (2009)
9. Y. Kolesnikov, C. Karcher, A. Thess, Lorentz force flowmeter for liquid aluminum: laboratory experiments and plant tests. Metall. Mater. Trans. B **42**, 441–450 (2011). https://doi.org/10.1007/s11663-011-9477-6
10. G. Janeschitz, Plasma–wall interaction issues in ITER. J. Nucl. Mater. **290**, 1–11 (2001). https://doi.org/10.1016/S0022-3115(00)00623-1
11. G. Kalinin, V. Barabash, A. Cardella et al., Assessment and selection of materials for ITER in-vessel components. J. Nucl. Mater. **283**, 10–19 (2000). https://doi.org/10.1016/S0022-3115(00)00305-6
12. J. Roth, E. Tsitrone, A. Loarte et al., Recent analysis of key plasma wall interactions issues for ITER. J. Nucl. Mater. **S390–S391**, 1–9 (2009). https://doi.org/10.1016/j.jnucmat.2009.01.037
13. K. Ikeda, Progress in the ITER physics basis—preface. Nucl. Fusion **47**, 1–24 (2007)
14. R. Hemsworth, H. Decamps, J. Graceffa et al., Status of the ITER heating neutral beam system. Nucl. Fusion **49**, 045006 (2009). https://doi.org/10.1088/0029-5515/49/4/045006
15. Q. Wang, *Practical Design of Magnetostatic Structure Using Numerical Simulation* (Wiley, Singapore, 2013)
16. S.D. Likhite, C. Radhakrishnamurty, P.W. Sahasrabudhe, Alternating current electromagnet hysteresis loop tracer for minerals and rocks. Rev. Sci. Instrum. **36**(11), 1558–1560 (1965). https://doi.org/10.1063/1.1719392